Sublimable Single Ion Magnets based on Lanthanoid Quinolinate Complexes: the Role of Intermolecular Interactions on their Thermal Stability

Walter Cañon-Mancisidor,[1,2,3*] Sara G. Miralles,[1] José J. Baldoví,[4] Guillermo Mínguez Espallargas,[1] Alejandro Gaita-Ariño,[1] Eugenio Coronado[1*]

[1] Instituto de Ciencia Molecular (ICMol), Universitat de València, c/ Catedrático José Beltrán, 2, E-46980 Paterna, Spain.

[2] Facultad de Química y Biología, Depto. de Química de los Materiales, Universidad de Santiago de Chile, USACH, Av. Lib Bernardo O´Higgins 3363, Estación Central, CP-9170022, Chile.

[3] Center for the Development of Nanoscience and Nanotechnology, CEDENNA, Av. Lib Bernardo O´Higgins 3363, Estación Central, CP-9170022, Chile.

[4] Max Planck Institute for the Structure and Dynamics of Matter, Luruper Chaussee 149, D-22761 Hamburg, Germany.

KEYWORDS Quinoline complexes, molecular magnetism, sublimable molecules, molecular spintronics.

ABSTRACT: We report the design, preparation and characterization of two families of thermally robust coordination complexes based on lanthanoid quinolinate compounds: $[Ln(5,7\text{-}Br_2q)_4]^-$ and $[Ln(5,7\text{-}ClIq)_4]^-$, where q = 8-hydroxyquinoline and Ln = Dy^{III}, Tb^{III}, Er^{III} and Ho^{III}. Samples of $[Dy(5,7\text{-}Br_2q)_4]^-$ decompose upon sublimation, whereas the sodium salt of $[Dy(5,7\text{-}ClIq)_4]^-$, which displays subtly different crystalline interactions, is sublimable under gentle conditions. The resulting film presents low roughness with high coverage and the molecular integrity of the coordination complex is verified through AFM, MALDI-TOF, FT-IR and microanalysis. Crucially, the single-molecule magnet behavior exhibited by $[Dy(5,7\text{-}ClIq)_4]^-$ in bulk remains detectable by ac magnetometry in the sublimated film.

1. INTRODUCTION

The ultimate miniaturization limit of nanospintronics is the manipulation of a single electron spin.[1] Mononuclear single-molecule magnets (SMMs), also called single ion magnets (SIMs),[2–8] are ideal systems on which to exert such a control and, thus, attractive candidates to be used as building blocks for spintronics and quantum computing applications.[9–16] These molecular nanomagnets are coordination compounds with a spin that resides in a single metal ion, displaying slow relaxation of the magnetization at low temperatures, together with quantum phenomena.[17,18] However, in order to exploit the possibilities of such magnetic entities in spintronics, they need to be processed into devices. This has motivated research aimed at the organization of SIMs, either in three dimensions[19] or, more commonly, in two dimensions.[10,20–26] Here the key point for the obtaining of useful devices is to design molecular nanomagnets that can be processed without losing the properties of interest.[27,28] A straightforward strategy towards this goal consists in obtaining magnetic molecules that are chemically stable upon sublimation.[10,24–28]

In this context, quinoline-based materials stand out as promising compounds for the development of optoelectronic[29,30] and magnetic devices.[31] In particular, the preparation of mononuclear lanthanoid-quinoline compounds of type $NaLnq_4$, where q = 8-hydroxyquinoline, which are the magnetic analogues of the extensively used Alq_3,[32] have been found to display a rich chemistry.[24,28–32] Surprisingly, these salts, formed by the anion $[Lnq_4]^-$ that electrostatically interacts with a Na^+ counter-cation, tend to be non-hygroscopic, air-stable and sublimable without decomposition. In this work, we have designed and prepared two families of potential mononuclear lanthanoid quinolinate SIMs: $[Ln(5,7\text{-}Br_2q)_4]^-$ and $[Ln(5,7\text{-}ClIq)_4]^-$. Both of them present a nearly isostructural coordination environment around the lanthanoid but differ in the substituents of the quinolinolate: 5,7-dibromo-8-hydroxyquinolinate and 5,7-chloroiodo-8-hydroxyquinolinate, respectively. As we will discuss, such a difference can influence intermolecular interactions, which in turn determine the possibilities for sublimation of different complexes and their potential use in the fabrication of nanodevices.

2. RESULTS AND DISCUSSION

2.1. Synthesis and structural characterization

Low crystallinity or even amorphous samples of both families, $Na[Ln(5,7\text{-}Br_2q)_4]$ **(1)** and $Na[Ln(5,7\text{-}ClIq)_4]$ **(2)** (Ln= Dy^{III}, Tb^{III}, Er^{III} and Ho^{III}), were obtained by direct reaction of the ligand with the corresponding $LnCl_3.6H_2O$ salt, as detailed in Supporting Information (Figures S11 and S12). Recrystallization in DMF resulted in single crystals of $Na[Ln(5,7\text{-}Br_2q)_4]\cdot DMF$ (**1-DMF**) and $Na[Ln(5,7\text{-}ClIq)_4]\cdot DMF$ (**2-DMF**). The structure and composition of the

samples were characterized by Fourier transform infrared spectroscopy (FTIR), electrospray ionization mass spectrometry (ES-MS), elemental analysis (EA), electron probe microanalysis (EPMA), thermogravimetry (TG) and X-ray powder diffraction Measurements (XPD) (see sections S.1.1-S.1.6 and S.3 in the Supporting Information). This multi-technique characterization confirms the same molecular entity before and after recrystallization. Additionally, crystals of the series **1-DMF** and **2-DMF** were studied by single crystal X-ray diffraction (SXRD) (section S2). Both molecular structures can be seen in Figure 1.

The coordination environments of **1-DMF** and **2-DMF** derivatives were described using the SHAPE code.[38,39] The results reveal that both of them show highly distorted geometries, which are closer to three different geometries (bicapped trigonal prism; square antiprism and triangular dodecahedron) (Figure S10). Such geometries are very common between *f*-block SIMs[40–44] and, in fact, lanthanoid-quinolinate complexes exhibiting SMM behavior with a very similar distorted square-antiprismatic geometry have previously been reported.[45,46]

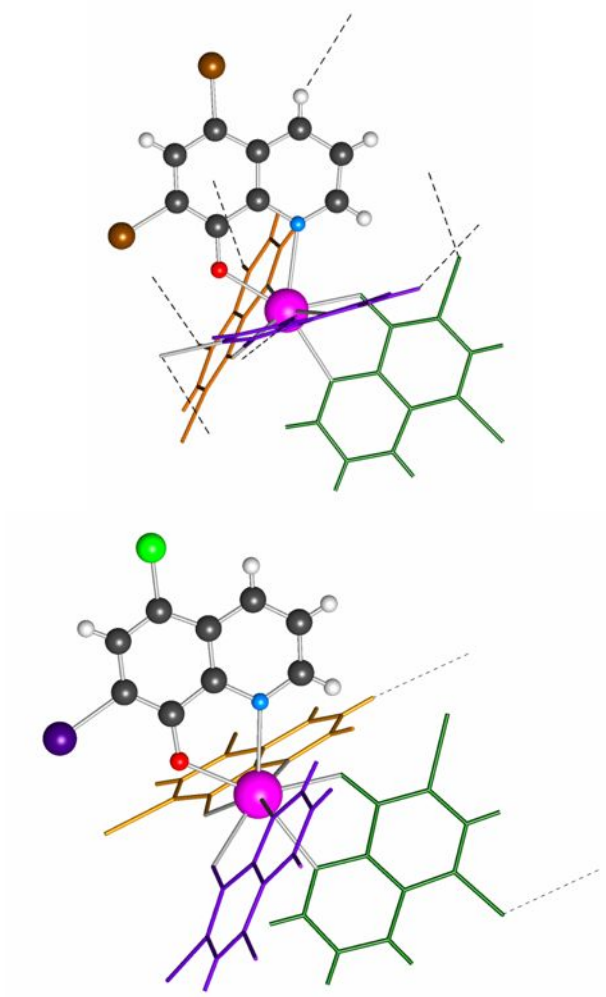

Figure 1. X-ray structure of $Na[Dy(5,7\text{-}Br_2q)_4]\cdot DMF$ (**1-DMF(Dy)**, up) and $Na[Dy(5,7\text{-}ClIq)_4]\cdot DMF$ (**2-DMF(Dy)**, down). Color labelling Pink: Dy, black: C, red: O, blue: N, light green: Cl, brown: Br, purple: I. The other three independent crystallographic quinolinates are represented in colors yellow, purple and green for clarity. Hydrogen bonds contact are represented as dotted lines. Na^+ has been omitted for clarity.

Moreover, in the crystal structures of the two series the most relevant common feature is that the closest Na^+ cation is coordinated by three oxygen atoms and two halogen atoms from the anionic complex (Figures S8 and S9). The coordination sphere of the Na^+ cation is completed by a DMF oxygen. This means that the crystal contains robust neutral supramolecular moieties with the potential to sublimate in gentle conditions; fine details of the packing should determine whether this potential is realized. Indeed, a striking difference between the crystal structures is the fact that the supramolecular moiety in **1-DMF** is bound to the crystal by up to 10 hydrogen bonds: 2 of type H··O and 8 of type H··Br. In contrast, the supramolecular moiety in **2-DMF** only displays 2 hydrogen bonds (of type H··Cl) to the rest of the crystal. Together with the lower crystallinity of **2**, this lets one expect an easier sublimation of the chloro-iodo derivative (Table S5). Thermogravimetry (Figure S7) seems to confirm these expectations, with near-vertical slopes below 400ºC in **2** and **2-DMF** –especially in the former– and a more gradual decomposition in the case of the dibrominated derivatives **1** and **1-DMF**.

2.2. Magnetic characterization of the bulk

We initiate the magnetic study with the systems with structural information, i.e. **1-DMF** and **2-DMF**, from which a magneto-structural correlation can be performed. Ground crystals of **1-DMF** and **2-DMF** (Ln = Dy, Tb, Ho, Er) were first characterized by static (dc) magnetic susceptibility measurements. The $\chi_M T$ values decrease at low temperatures due to the thermal depopulation of the Stark sublevels. For the Er complexes, the fast decrease of the $\chi_M T$ values observed below 100 K, compared to the other lanthanoids, can be related to the different sign of the second order Stevens parameter, resulting in a stabilization of the low m_J doublets for Er, whereas for Dy, Tb and Ho, the high m_J ground states are stabilized. We used the *semi-empirical* Radial Effective Charge[47] (REC) model implemented in the SIMPRE package[48–50] to relate the measured magnetic properties with the energy level scheme and the nature of the ground state of each of these complexes (see section S.4.2 in the Supp. Information for details). A collective fit of the temperature dependence of the magnetic susceptibility of the four derivatives of each family was employed (Figure 2). Magnetization curves of **1-DMF(Dy)** and **2-DMF(Dy)** present butterfly hysteresis (Figure S14), suggesting the presence of slow-magnetic relaxation, as also observed for other lanthanide SIMs.[6]

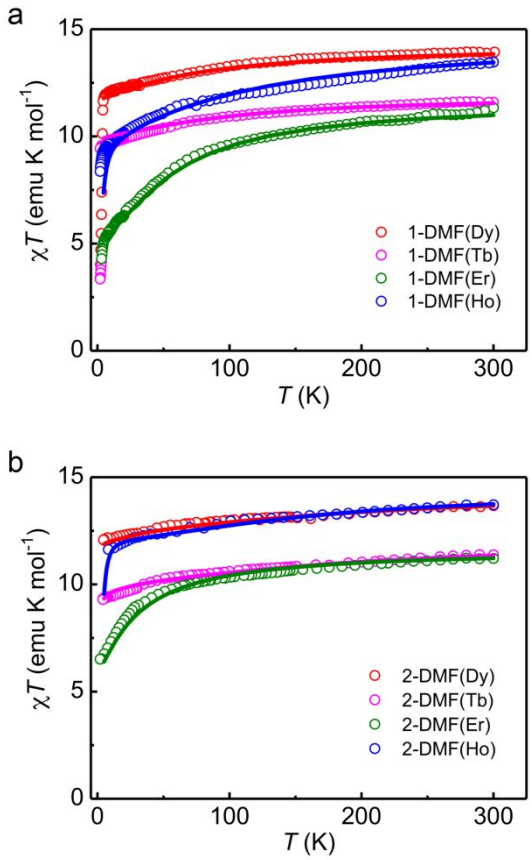

Figure 2. Calculated and experimental χT product from 2 to 300 K of compounds **1-DMF** (a) and **2-DMF** (b). Tb (pink), Dy (red), Ho (blue) and Er (green).

According to these calculations, both Dy derivatives have their ground state functions mainly characterized by M_J = ±15/2, with 84% and 96% contributions for **1-DMF(Dy)** and **2-DMF(Dy)**, respectively. In both complexes, the first excited state appears at a sufficiently high energy, which in principle should favor slow relaxation of the magnetization at low temperature. These calculations may also anticipate SMM behavior in the Tb derivatives, although ground doublets with tunneling splittings of 0.4 and 1.9 cm^{-1} are predicted. Their calculated ground states exhibit important mixing of M_J = +6 and M_J = -6, with weights of over 40% each. Consequently, longitudinal magnetic field is needed in order to cancel this mixture and to obtain states that can be characterized as M_J = +6 and M_J = -6 respectively, see Figure 3.

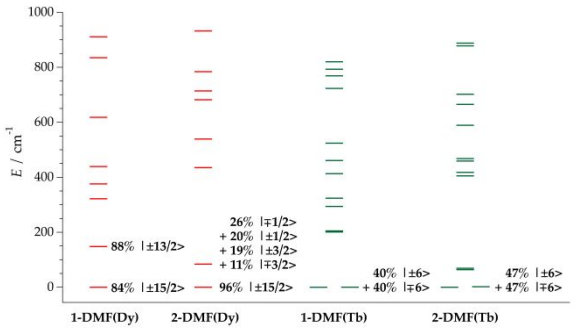

Figure 3. Calculated energy level scheme and main M_J contributions to the ground state for the Dy^{III} and Tb^{III} complexes of **1-DMF** and **2-DMF**.

The magnetic characterization of **1-DMF(Dy)** and **2-DMF(Dy)** was completed by alternate current (ac) measurements. Both present frequency-dependent peaks but no maxima appear above 2 K unless an external field is applied for **1-DMF(Dy)**. In contrast, maxima appears at high frequencies for **2-DMF(Dy)** at zero dc field, which allows the possibility of obtained an U_{eff} value of 52 cm^{-1} that is slightly lower than the value of 54 cm^{-1} of **1-DMF(Dy)** obtained by extrapolation of U_{eff} at different dc fields (See section S.4.3.). For illustration we focus here on **2-DMF(Dy)**, but qualitatively the same results are found for **1-DMF(Dy)** (Figure 4 and details in the ESI, including Figures S15-S27).[19,51] The magnetic dynamics were analyzed under the optimal field H_{dc} = 500 G, aiming to decide between Raman vs Orbach processes for the magnetic relaxation. Whereas high-temperature data can be fitted assuming an Orbach mechanism (U_{eff} = 76 ± 3 cm^{-1}), the Raman-only fit provides an excellent fit for the whole temperature range, with $B_{Raman} = (6.9 \pm 0.3) \cdot 10^{-9}$ Hz/K^9, with no need for a fit that allows both mechanisms. At least under an applied field of 500 G and up to 20K and 10000 Hz, we can conclude that both for **1-DMF(Dy)** and **2-DMF(Dy)** a Raman mechanism is in operation and no real energy levels participate in the magnetic relaxation. Moreover, we cannot exclude the important role of vibrations in the spin relaxation of SMMs, which was recently analyzed by some of us[52]. The ac measurements of **1-DMF(Tb)**, **2-DMF(Tb)**, **1-DMF(Er)** and **2-DMF(Er)** are presented in the Supporting Information (Figures S28 to S31), revealing a maximum in the out-of-phase signal only at the highest frequency with an external applied dc field.

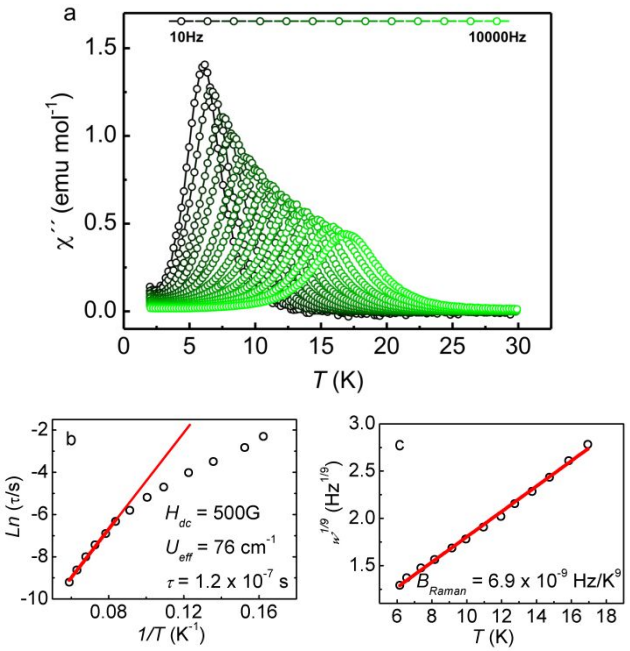

Figure 4. (a) Out-phase ac susceptibility measurements at H_{dc} = 500 G for **2-DMF(Dy)**. (b,c) Best-fit of the ac data assuming an Orbach (b) and Raman (c) relaxation processes.

2.3. Film fabrication

In order to study the suitability of these SIMs for device fabrication, we tested the samples with the best SMM behavior (**1(Dy)**, **2(Dy)**, **1-DMF(Dy)**, **2-DMF(Dy)**) for sublimation. Samples of the four systems were evaporated under the same experimental conditions (a base pressure between 10^{-6} and 10^{-7}

mbar) and in a temperature range between 180 and 200 °C for **1(Dy)** and **1-DMF(Dy)**, and between 220 and 240 °C in the case of **2(Dy)** and **2-DMF(Dy)**, onto a glass substrate. The deposited materials were studied with an array of characterization techniques including surface XRD (SXRD), MALDI-TOF, FTIR and EDAX (see section S.5.2 in the Supporting Information), in order to determine if the chemical composition of the material was maintained upon sublimation. As expected from TG, both **2(Dy)** and **2-DMF(Dy)** were found to be suitable for sublimation, obtaining yellow translucent films deposited on the glass substrate (Figure S32) while **1(Dy)** and **1-DMF(Dy)** decomposed. Both films, formed either using **2(Dy)** or **2-DMF(Dy)** as starting materials, are amorphous (Figure S35), but possess the same composition (Table S14). The molecular integrity of the chlorinated-iodinated complexes was confirmed to be maintained by IR (Figure S34) and the MALDI-TOF isotopical profiles, which match with the theoretical predictions (Figures 5 and S33). For the two films, it is possible to observe in the negative mode that the experimental patterns match with the theoretical predictions for the anion, $[Dy(5,7\text{-}ClIq)_4]^-$ at m/Z = 1380. In the positive mode a pattern corresponding to the $Na_2[Dy(5,7\text{-}ClIq)_4]^+$ fragment is observed at m/Z = 1425. Moreover, the correct atomic relation between the lanthanoid and both Cl and I was obtained by electron probe microanalysis, Dy: Cl: I = 1: 4: 4 (Table S14). Thus, upon sublimation, the recrystallized phase (**2-DMF(Dy)**) loses the solvent molecule (DMF) at a temperature below the temperature of sublimation, but the deposited material contains the same magnetic molecule as **2-(Dy)**, $Na[Dy(5,7\text{-}ClIq)_4]$, as confirmed by MALDI-TOF measurements.

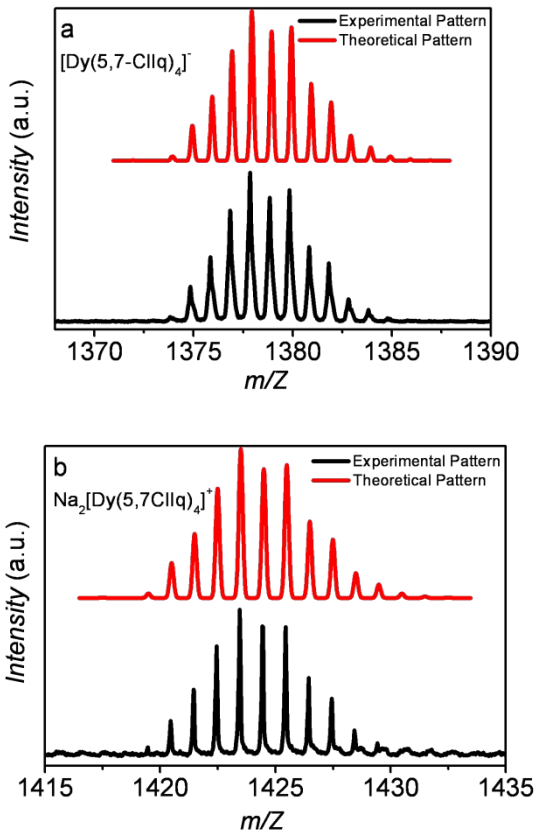

Figure 5. Experimental (black) versus theoretical (red) isotopical profiles obtained by MALDI-TOF in negative (a) and positive (b) modes of the deposited material obtained by sublimation of $Na[Dy(5,7\text{-}ClIq)_4]$, **2(Dy)**.

The difference in sublimability in these two near-isostructural complexes might not be unambiguously traced back to differences in the crystal packing, since the sublimation of the crystals coincide with those of the amorphous samples[53]. Presumably, the different behavior is related to the different interactions that are possible in chlorinaded-iodinated derivatives compared with dibrominated derivatives, due to the different polarizabilities and electronegativities of the different halogens. In any case, the behavior is consistent with available experimental data as presented above: before crystallization, **1(Dy)** is much more crystalline than **2(Dy)**, and after crystallization, **1-DMF(Dy)** presents a higher number of hydrogen bonds compared with **2-DMF(Dy)**.

To characterize the topography of the deposited material, sublimated films of 20 nm of **2(Dy)** on glass substrates were imaged by AFM. The image showed that the sublimated material forms small aggregates a few nanometers thick, uniformly covering the substrate. The film of **2(Dy)** in a window of 1μm x 1μm had an estimated peak to peak value of 17.2 nm with a low *RMS* roughness of 1.34 nm and roughness average of 0.80 nm. Figure 6 shows the AFM image of **2(Dy)** together with the profile and topography of the film. AFM topography images show low roughness and uniform films, characteristics that make this material suitable for placing them in heterostructures.

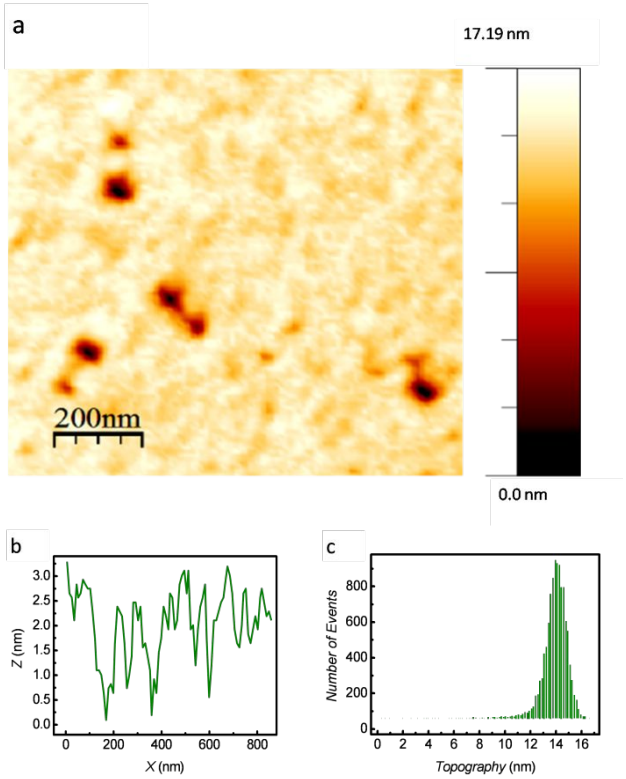

Figure 6. Topographic characterization of sublimated **2(Dy)**. (a) AFM image (1μm x 1μm). (b) Profile of the sublimated film. (c) topography of the sublimated film.

In order to observe if the magnetic properties of **2(Dy)** and **2-DMF(Dy)** are maintained after sublimation, *ac* susceptibility was measured using a SQUID magnetometer at different frequencies under an applied magnetic field H_{dc} = 500 G in a temperature range of 2 – 30 K. Figure S36 shows the

comparison of the re-crystallized material (**2-DMF(Dy)**), the non-recrystallized material (**2(Dy)**) and the evaporate material of **2(Dy).** In-phase and out-of-phase magnetic susceptibilities show frequency dependent signals with differences in the maximum temperatures of 1.5 K moving to lower temperatures for the compounds without DMF.

The dynamic magnetic properties were measured on deposited material (1 mg) that was obtained after several evaporations in order to form a thick film of **2(Dy)**. Dynamic magnetometry reveals that there is frequency dependence in the in- and out-phase susceptibilities. At H_{dc} = 500 G clear maxima can be observed in both χ' and χ'' allowing the study of the relaxation of the system (see Figures 7 and S36).

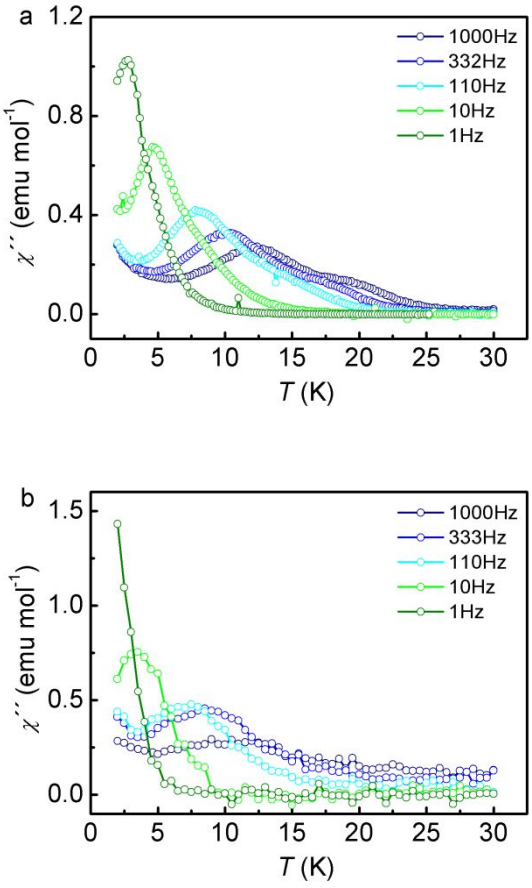

Figure 7. Out-of-phase susceptibility measurements of **2(Dy)** under an external field H_{dc} = 500 G (a) powder sample and (b) film sample.

A comparison between the powder and the film samples of the dynamic magnetic properties of **2(Dy)** is plotted in Figure 7. We observed that these properties are very similar, indicating that molecular structure of the complex is maintained after the sublimation process. This close similarity can also be seen in the analysis of the relaxation mechanism extracted from the magnetic data. Thus, assuming a Raman process, the value of the B_{Raman} constant is very close in both cases ($(1.4 \pm 0.7)\cdot10^{-9}$ Hz/K^9 for the film and $(4.4 \pm 2.1)\cdot10^{-9}$ Hz/K^9 for the powder). Also, an Orbach relaxation mechanism in the high temperature range affords an identical, within experimental error, energy barrier for the film (U_{eff} = 29.7 ± 1.7 cm^{-1}) and the powder (U_{eff} = 30 ± 3 cm^{-1}). (See Figure 8).

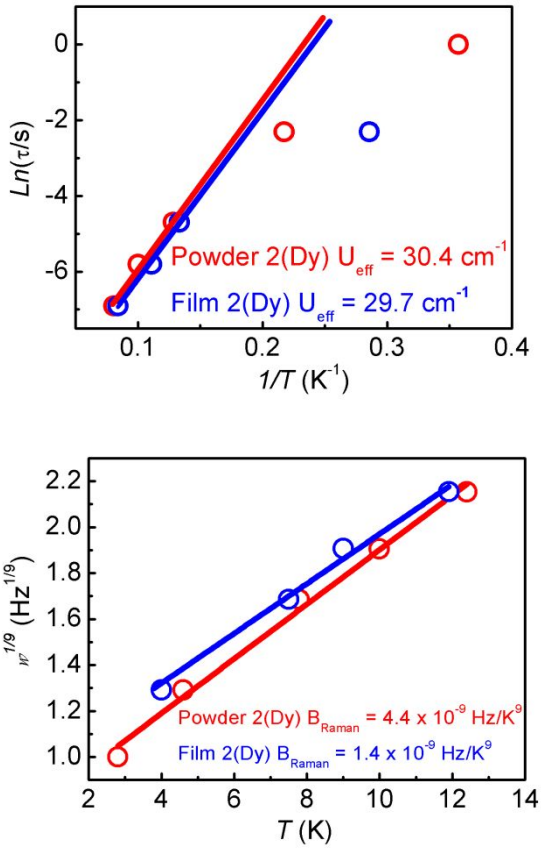

Figure 8. Orbach (Ln(τ) vs *1/T*) and Raman ($w^{1/9}$ vs *T*) relaxation studies of **2(Dy)**.

3. CONCLUSIONS

Two families of quinoline based mononuclear lanthanoid complexes have been synthesized, namely $[Ln(5,7\text{-}Br_2q)_4]^-$ and $[Ln(5,7\text{-}ClIq)_4]^-$ (**1** and **2**, respectively). Recrystallization in DMF allows their structural elucidation. In both cases, a robust neutral moiety including a firmly bound sodium counter-cation points towards a potential for sublimation. Intermolecular hydrogen bonds are an important difference between the two series, with the neutral moiety in the dibrominated derivative being more strongly attached to the rest of the crystalline lattice, contrary to the chloro-iodine derivative, which presents considerably less intermolecular interaction, being the reason why **2-DMF(Dy)** is the system that can be sublimed.

Furthermore, we have been able to perform a systematic study of different changes that influence the magnetic properties: i) the lanthanoid center; ii) the first coordination sphere (through changes in the halogen substituents in the organic ligand); iii) the second coordination sphere (through changes in the solvation molecules and crystallinity).

The dc magnetic properties are well described by the theoretical characterization, which explained the SMM behavior of the Dy^{III} and Tb^{III} complexes. Of these series of compounds, dysprosium complexes present SIM behavior independently of the applied dc field. Terbium compounds also exhibit SMM behavior but only with a dc field of at least 1500 G. For the dysprosium complexes, Raman relaxation mechanism is dominant and masks the Orbach mechanism. However, this does not mean that Orbach relaxation is not present.

In addition, the zero-dc-field energy barrier of the relaxation of the magnetization for **1-DMF(Dy)** and for **2-DMF(Dy)** reflect that the halogen substituent in the quinolinate ligands affects slightly the magnetic properties. (U_{eff} = 54 cm^{-1} and U_{eff} = 52 cm^{-1} for **1-DMF(Dy)** and **2-DMF(Dy)**, respectively). At high temperatures lineal fits are obtained using Arrhenius plot for both cases, which agrees with an Orbach process

Finally, the changes in the second coordination sphere of the lanthanoid center have been analyzed through comparison of solvated and unsolvated complexes **2(Dy)** and **2-DMF(Dy)**. This shows the combined effect on the magnetic relaxation of the presence/absence of coordinated solvent molecules to the Na^+ cation and the differences in crystallinity. Values of U_{eff} = 30 cm^{-1} and α = 0.28 for **2 (Dy)**, and U_{eff} = 52 cm^{-1} (α = 0.05) for **2-DMF(Dy)** are obtained under a dc field of 500G.

To summarize, the main conclusion of this work is that we achieve sublimable SIMs through the use of intermolecular interactions to modulate the thermal stability. This makes this system very interesting for integration in spintronic devices. [54]

EXPERIMENTAL

A modified approach of the synthesis of lanthanide tetrakis complexes described by Van Deun and others[29,33,36] was used to obtain a family of pure tetrakis complexes of general formula, $Na[Ln(5,7\text{-}X_2q)_4]$, where the ligands are 5,7-dibromo-8-hydroxyquinoline (5,7-Br_2q) and 5,7-chloroiodo-8-hydroxyquinoline (5,7-ClIq), see Section S.1.1. to S.1.3. in the supporting information.

Compound Physical Characterization

Several experimental techniques were used to characterized the compounds such as; Fourier transform infrared spectroscopy (FTIR); ESI-mass spectra; elemental analysis (C, N, H); electron probe microanalysis (EPMA); thermal analysis; X-ray Powder Diffraction Measurements (XPD); Single crystal X-ray diffraction (SXRD). Single crystals of compounds **1-DMF (Ln = Dy, Tb**, **Er**, **Ho)** and **2-DMF (Ln = Dy, Tb**, **Er**, **Ho)** were measured. A summary of the data collection and structure refinements is provided in Tables S1 and S2. CCDC-1562344 to -1562351 contains the supplementary crystallographic data for this paper. These data can be obtained free of charge from The Cambridge Crystallographic Data Centre via www.ccdc.cam.ac.uk/data_request/cif.

Magnetic susceptibility measurements (dc and ac) were done for all compounds (see ESI for more information, Figures 2 and S14 to S31).

Film Physical Characterization

For the film fabrication, glass substrates of 3 cm x 3 cm were transferred to a vacuum chamber and evacuated to a pressure between 10^{-6} – 10^{-7} mbar. A ceramic crucible was filled with compounds **1(Dy)**, **1-DMF(Dy)**, **2(Dy)** and **2-DMF(Dy)**, and then were heated between 190 to 240 °C. The film thickness was controlled by the rate of evaporation of 0.1 Å/s to a thickness of 20 nm, since a calibration was made using an Ambios Technology XP-1 perfilometer placed on a vibration isolation table. The films were characterized by Fourier transform infrared spectroscopy (FTIR) and Matrix-Assisted Laser Desorption /Ionization Time of Flight Mass Spectrometry (MALDI-TOF). We performed the MALDI-TOF without matrix as the presence of the matrix prevented the observation of the molecular pattern. The Ln : X ratios (where X = Br, I, Cl) of the film samples were estimated by electron probe microanalysis (EPMA). Surface diffraction to the sublimated films of the compounds **2(Dy)** and **2-DMF(Dy)** at room temperature between 10° to 40° (*2θ*) were done. AFM measurements, a Nanoscope Multimode (Veeco) atomic force microscope in tapping mode operation was used in the morphological study. Film magnetic susceptibility measurements were done for **2(Dy)** in a Quantum Design MPMS XL-5 SQUID (see Section S.5. in the supporting information).

ASSOCIATED CONTENT

Supporting Information Available: The supporting information is available free of charge via the Internet at http://pubs.acs.org. A detail explanation of the Synthesis, Experimental, Compound Characterization, FTIR, Thermal Properties, PXRD, SXRD, dc Magnetic Susceptibility, ac Magnetic Susceptibility, Film Fabrication, Film Characterization and Magnetic Properties of the Film is presented in the supporting information.

AUTHOR INFORMATION

Corresponding Authors
E-Mail for W.C.M.: walter.canon@usach.cl
E-Mail for E.C.: eugenio.coronado@uv.es

ACKNOWLEDGEMENTS

The present work has been funded by the EU (ERC Advanced Grant Mol2D 788222) and ERC Consolidator Grants DECRESIM (647301) and COSMICS (766726)), the Spanish MINECO (grant MAT2017-89993-R, CTQ2014-52758-P, CTQ2014-59209-P and 'Unidad de Excelencia María de Maeztu' MDM-2015-0538 granted to ICMol), and the Generalitat Valenciana (Prometeo Program of excellence). A.G.-A. and G.M.E acknowledge funding by the MINECO (Ramón y Cajal contracts). J.J.B. thanks the EU for for a Marie Curie Fellowship (H2020-MSCA-IF-2016-751047). S.G.M. thanks the Spanish MINECO for a FPI predoctoral grant. WCM thanks FONDECYT de Iniciación 11160830 for financial support and Redes Internacionales para Investigadores en Etapa Inicial, REDI170277. MALDI-TOF was performed in the Proteomics Unit of SCSIE University of Valencia that belongs to ProteoRed, PRB2-ISCIII, supported by grant PT13/0001.

REFERENCES

(1) Wolf, S. A.; Awschalom, D. D.; Buhrman, R. A.; Daughton, J. M.; von Molnár, S.; Roukes, M. L.; Chtchelkanova, A. Y.; Treger, D. M. Spintronics: A Spin-Based Electronics Vision for the Future. *Science* **2001**, *294*, 1488–1495

(2) Ishikawa, N.; Sugita, M.; Ishikawa, T.; Koshihara, S. Y.; Kaizu, Y. Lanthanide Double-Decker Complexes Functioning as Magnets at the Single-Molecular Level. *J. Am. Chem. Soc.* **2003**, *125*, 8694–8695.

(3) AlDamen, M. A.; Clemente-Juan, J. M.; Coronado, E.; Martí-Gastaldo, C.; Gaita-Ariño, A. Mononuclear Lanthanide Single-Molecule Magnets Based on Polyoxometalates. *J. Am. Chem. Soc.* **2008**, *130*, 8874–8875.

(4) Jiang, S. Da; Wang, B. W.; Su, G.; Wang, Z. M.; Gao, S. A Mononuclear Dysprosium Complex Featuring Single-Molecule-Magnet Behavior. *Angew. Chemie Int. Ed.* **2010**, *49*, 7448–7451.

(5) Jiang, S. Da; Wang, B. W.; Sun, H. L.; Wang, Z. M.; Gao, S. An Organometallic Single-Ion Magnet. *J. Am. Chem. Soc.* **2011**, *133*, 4730–4733.

(6) Woodruff, D. N.; Winpenny, R. E. P.; Layfield, R. A. Lanthanide Single-Molecule Magnets. *Chem. Rev.* **2013**, *113*, 5110–5148.

(7) Goodwin, C. A. P.; Ortu, F.; Reta, D.; Chilton, N. F.; Mills, D. P. Molecular Magnetic Hysteresis at 60 Kelvin in Dysprosocenium. *Nature* **2017**, *548*, 439–442.

(8) Guo, F.-S.; Day, B. M.; Chen, Y.-C.; Tong, M.-L.; Mansikkamäki, A.; Layfield, R. A. A Dysprosium Metallocene Single-Molecule Magnet Functioning at the Axial Limit. *Angew. Chemie Int. Ed.* **2017**, *56*, 11445–11449.

(9) Urdampilleta, M.; Klyatskaya, S.; Cleuziou, J.-P.; Ruben, M.; Wernsdorfer, W. Supramolecular Spin Valves. *Nat. Mater.* **2011**, *10*, 502–506.

(10) Komeda, T.; Isshiki, H.; Liu, J.; Zhang, Y.-F.; Lorente, N.; Katoh, K.; Breedlove, B. K.; Yamashita, M. Observation and Electric Current Control of a Local Spin in a Single-Molecule Magnet. *Nat. Commun.* **2011**, *2*, 217.

(11) Bogani, L.; Wernsdorfer, W. Molecular Spintronics Using Single-Molecule Magnets. *Nat. Mater.* **2008**, *7*, 179–186.

(12) Martínez-Pérez, M. J.; Cardona-Serra, S.; Schlegel, C.; Moro, F.; Alonso, P. J.; Prima-García, H.; Clemente-Juan, J. M.; Evangelisti, M.; Gaita-Ariño, A.; Sesé, J.; Van Slageren, J.; Coronado, E.; Luis, F. Gd-Based Single-Ion Magnets with Tunable Magnetic Anisotropy: Molecular Design of Spin Qubits. *Phys. Rev. Lett.* **2012**, *108*, 247213.

(13) Leuenberger, M. N.; Loss, D. Quantum Computing in Molecular Magnets. *Nature* **2001**, *410*, 789–793.

(14) Clemente-Juan, J. M.; Coronado, E.; Gaita-Ariño, A. Magnetic Polyoxometalates: From Molecular Magnetism to Molecular Spintronics and Quantum Computing. *Chem. Soc. Rev.* **2012**, *41*, 7464–7478.

(15) Bertaina, S.; Gambarelli, S.; Tkachuk, A.; Kurkin, I. N.; Malkin, B.; Stepanov, A.; Barbara, B. Rare-Earth Solid-State Qubits. *Nat. Nanotechnol.* **2007**, *2*, 39–42.

(16) Stamp, P. C. E.; Gaita-Ariño, A. Spin-Based Quantum Computers Made by Chemistry: Hows and Whys. *J. Mater. Chem.* **2008**, *19*, 1718–1730.

(17) Gatteschi, D.; Sessoli, R. Quantum Tunneling of Magnetization and Related Phenomena in Molecular Materials. *Angew. Chemie Int. Ed.* **2003**, *42*, 268–297.

(18) Troiani, F.; Affronte, M. Molecular Spins for Quantum Information Technologies. *Chem. Soc. Rev.* **2011**, *40*, 3119–3129.

(19) Baldoví, J. J.; Coronado, E.; Gaita-Ariño, A.; Gamer, C.; Giménez-Marqués, M.; Mínguez Espallargas, G. A SIM-MOF: Three-Dimensional Organisation of Single-Ion Magnets with Anion-Exchange Capabilities. *Chem. - A Eur. J.* **2014**, *20*, 10695–10702.

(20) Mannini, M.; Bonacchi, D.; Zobbi, L.; Piras, F. M.; Speets, E. A.; Caneschi, A.; Cornia, A.; Magnani, A.; Ravoo, B. J.; Reinhoudt, D. N.; Sessoli, R.; Gatteschi, D. Advances in Single-Molecule Magnet Surface Patterning through Microcontact Printing. *Nano Lett.* **2005**, *5*, 1435–1438.

(21) Mannini, M.; Pineider, F.; Sainctavit, P.; Danieli, C.; Otero, E.; Sciancalepore, C.; Talarico, A. M.; Arrio, M.-A.; Cornia, A.; Gatteschi, D.; Sessoli, R. Magnetic Memory of a Single-Molecule Quantum Magnet Wired to a Gold Surface. *Nat. Mater.* **2009**, *8*, 194–197.

(22) Gonidec, M.; Biagi, R.; Corradini, V.; Moro, F.; De Renzi, V.; Del Pennino, U.; Summa, D.; Muccioli, L.; Zannoni, C.; Amabilino, D. B.; Veciana, J. Surface Supramolecular Organization of a Terbium(III) Double-Decker Complex on Graphite and Its Single Molecule Magnet Behavior. *J. Am. Chem. Soc.* **2011**, *133*, 6603–6612.

(23) Mannini, M.; Bertani, F.; Tudisco, C.; Malavolti, L.; Poggini, L.; Misztal, K.; Menozzi, D.; Motta, A.; Otero, E.; Ohresser, P.; Sainctavit, P.; Condorelli, G. G.; Dalcanale, E.; Sessoli, R. Magnetic Behaviour of $TbPc_2$ Single-Molecule Magnets Chemically Grafted on Silicon Surface. *Nat. Commun.* **2014**, *5*, 4582.

(24) Malavolti, L.; Poggini, L.; Margheriti, L.; Chiappe, D.; Graziosi, P.; Cortigiani, B.; Lanzilotto, V.; Buatier de Mongeot, F.; Ohresser, P.; Otero, E.; Choueikani, F.; Sainctavit, P.; Bergenti, I.; Dediu, V. A.; Mannini, M.; Sessoli, R. Magnetism of $TbPc_2$ SMMs on Ferromagnetic Electrodes Used in Organic Spintronics. *Chem. Commun.* **2013**, *49*, 11506–11508.

(25) Klar, D.; Candini, A.; Joly, L.; Klyatskaya, S.; Krumme, B.; Ohresser, P.; Kappler, J.-P.; Ruben, M.; Wende, H. Hysteretic Behaviour in a Vacuum Deposited Submonolayer of Single Ion Magnets. *Dalton Trans.* **2014**, *43*, 10686–10689.

(26) Katoh, K.; Isshiki, H.; Komeda, T.; Yamashita, M. Molecular Spintronics Based on Single-Molecule Magnets Composed of Multiple-Decker Phthalocyaninato Terbium(III) Complex. *Chem. - An Asian J.* **2012**, *7*, 1154–1169.

(27) Dreiser, J.; Pacchioni, G. E.; Donati, F.; Gragnaniello, L.; Cavallin, A.; Pedersen, K. S.; Bendix, J.; Delley, B.; Pivetta, M.; Rusponi, S.; Brune, H. Out-of-Plane Alignment of Er(Trensal) Easy Magnetization Axes Using Graphene. *ACS Nano* **2016**, *10*, 2887–2892.

(28) Kiefl, E.; Mannini, M.; Bernot, K.; Yi, X.; Amato, A.; Leviant, T.; Magnani, A.; Prokscha, T.; Suter, A.; Sessoli, R.; Salman, Z. Robust Magnetic Properties of a Sublimable Single-Molecule Magnet. *ACS Nano* **2016**, *10*, 5663–5669.

(29) Bisti, F.; Anemone, G.; Donarelli, M.; Penna, S.; Reale, A.; Ottaviano, L. Tetrakis Erbium Quinolinate Complexes , Electronic Structure Investigation. *Org. Electron.* **2014**, *15*, 1810–1814.

(30) Artizzu, F.; Mercuri, M. L.; Serpe, A.; Deplano, P. NIR-Emissive Erbium–Quinolinolate Complexes.

Coord. Chem. Rev. **2011**, *255*, 2514–2529.

(31) Bedoya-Pinto, A.; Prima-García, H.; Casanova, F.; Coronado, E.; Hueso, L. E. Spin-Polarized Hopping Transport in Magnetically Tunable Rare-Earth Quinolines. *Adv. Electron. Mater.* **2015**, 1500065.

(32) Thompson, J.; Blyth, R. I. R.; Gigli, G.; Cingolani, R. Obtaining Characteristic 4f-4f Luminescence from Rare Earth Organic Chelates. *Adv. Funct. Mater.* **2004**, *14*, 979–984.

(33) Van Deun, R.; Fias, P.; Nockemann, P.; Schepers, A.; Parac-Vogt, T. N.; Van Hecke, K.; Van Meervelt, L.; Binnemans, K. Rare-Earth Quinolinates: Infrared-Emitting Molecular Materials with a Rich Structural Chemistry. *Inorg. Chem.* **2004**, *43*, 8461–8469.

(34) Artizzu, F.; Bernot, K.; Caneschi, A.; Coronado, E.; Clemente-Juan, J. M.; Marchiò, L.; Mercuri, M. L.; Pilia, L.; Serpe, A.; Deplano, P. Synthesis, Structure, Spectroscopic Studies and Magnetic Properties of the Tetrakis(5,7-Dichloro-8-Quinolinolato)Gadolinium(III) Complex. *Eur. J. Inorg. Chem.* **2008**, 3820–3826.

(35) Artizzu, F.; Marchiò, L.; Mercuri, M. L.; Pilia, L.; Serpe, A.; Quochi, F.; Orrù, R.; Cordella, F.; Saba, M.; Mura, A.; Bongiovanni, G.; Deplano, P. New Insights on Near-Infrared Emitters Based on Er-Quinolinolate Complexes: Synthesis, Characterization, Structural, and Photophysical Properties. *Adv. Funct. Mater.* **2007**, *17*, 2365–2376.

(36) Camargo, H.; Paolini, T. B.; Niyama, E.; Brito, H. F.; Cremona, M. New Rare-Earth Quinolinate Complexes for Organic Light-Emitting Devices. *Thin Solid Films* **2013**, *528*, 36–41.

(37) O'Riordan, A.; Van Deun, R.; Mairiaux, E.; Moynihan, S.; Fias, P.; Nockemann, P.; Binnemans, K.; Redmond, G. Synthesis of a Neodymium-Quinolate Complex for near-Infrared Electroluminescence Applications. *Thin Solid Films* **2008**, *516*, 5098–5102.

(38) Casanova, D.; Cirera, J.; Llunell, M.; Alemany, P.; Avnir, D.; Alvarez, S. Minimal Distortion Pathways in Polyhedral Rearrangements. *J. Am. Chem. Soc.* **2004**, *126*, 1755–1763.

(39) Casanova, D.; Llunell, M.; Alemany, P.; Álvarez, S. The Rich Stereochemistry of Eight-Vertex Polyhedra: A Continuous Shape Measures Study. *Chem. - A Eur. J.* **2005**, *11*, 1479–1494.

(40) Kettles, F. J.; Milway, V. A.; Tuna, F.; Valiente, R.; Thomas, L. H.; Wernsdorfer, W.; Ochsenbein, S. T.; Murrie, M. Exchange Interactions at the Origin of Slow Relaxation of the Magnetization in $\{TbCu_3\}$ and $\{DyCu_3\}$ Single-Molecule Magnets. *Inorg. Chem.* **2014**, *53*, 8970–8978.

(41) Zhu, J.; Wang, C.; Luan, F.; Liu, T.; Yan, P.; Li, G. Local Coordination Geometry Perturbed β-Diketone Dysprosium Single-Ion Magnets. *Inorg. Chem.* **2014**, *53*, 8895–8901.

(42) Hänninen, M. M.; Mota, A. J.; Aravena, D.; Ruiz, E.; Sillanpää, R.; Camón, A.; Evangelisti, M.; Colacio, E. Two C3 -Symmetric Dy_3^{III} Complexes with Triple Di-μ-Methoxo-μ-Phenoxo Bridges, Magnetic Ground State, and Single-Molecule Magnetic Behavior. *Chem. - A Eur. J.* **2014**, *20*, 8410–8420.

(43) Li, X.; Wei, D. Y.; Huang, S. J.; Zheng, Y. Q. Syntheses and Characterization of Novel Lanthanide Adamantine-Dicarboxylate Coordination Complexes. *J. Solid State Chem.* **2009**, *182*, 95–101.

(44) Zhang, X. Q.; Lin, M. S.; Hu, B.; Chen, W. Q.; Zheng, L. N.; Wu, J.; Chen, Y. M.; Zhou, F. Y.; Li, Y. H.; Li, W. Anionic Lanthanide Complexes Supported by a Pyrrole-Based Tetradentate Schiff Base Ligand: Synthesis, Structures and Catalytic Activity toward the Polymerization of -Caprolactone. *Polyhedron* **2012**, *33*, 273–279.

(45) Chilton, N. F.; Deacon, G. B.; Gazukin, O.; Junk, P. C.; Kersting, B.; Langley, S. K.; Moubaraki, B.; Murray, K. S.; Schleife, F.; Shome, M.; Turner, D. R.; Walker, J. A. Structure, Magnetic Behavior, and Anisotropy of Homoleptic Trinuclear Lanthanoid 8-Quinolinolate Complexes. *Inorg. Chem.* **2014**, *53*, 2528–2534.

(46) Miralles, S. G.; Bedoya-Pinto, A.; Baldoví, J. J.; Cañon-Mancisidor, W.; Prado, Y.; Prima-Garcia, H.; Gaita-Ariño, A.; Mínguez Espallargas, G.; Hueso, L. E.; Coronado, E. Sublimable Chloroquinolinate Lanthanoid Single-Ion Magnets Deposited on Ferromagnetic Electrodes. *Chem. Sci.* **2018**, *9*, 199–208.

(47) Baldoví, J. J.; Borrás-Almenar, J. J.; Clemente-Juan, J. M.; Coronado, E.; Gaita-Ariño, A. Modeling the Properties of Lanthanoid Single-Ion Magnets Using an Effective Point-Charge Approach. *Dalton Trans.* **2012**, *41*, 13705.

(48) Baldoví, J. J.; Cardona-Serra, S.; Clemente-Juan, J. M.; Coronado, E.; Gaita-Ariño, A.; Palii, A. SIMPRE: A Software Package to Calculate Crystal Field Parameters, Energy Levels, and Magnetic Properties on Mononuclear Lanthanoid Complexes Based on Charge Distributions. *J. Comput. Chem.* **2013**, *34*, 1961–1967.

(49) Baldoví, J. J.; Gaita-Ariño, A.; Coronado, E. Modeling the Magnetic Properties of Lanthanide Complexes: Relationship of the REC Parameters with Pauling Electronegativity and Coordination Number. *Dalton Trans.* **2015**, *44*, 12535–12538.

(50) Baldoví, J. J.; Clemente-Juan, J. M.; Coronado, E.; Duan, Y.; Gaita-Ariño, A.; Giménez-Saiz, C. Construction of a General Library for the Rational Design of Nanomagnets and Spin Qubits Based on Mononuclear F-Block Complexes. The Polyoxometalate Case. *Inorg. Chem.* **2014**, *53*, 9976–9980.

(51) Ishikawa, N.; Sugita, M.; Wernsdorfer, W. Nuclear Spin Driven Quantum Tunneling of Magnetization in a New Lanthanide Single-Molecule Magnet: Bis(Phthalocyaninato)Holmium Anion. *J. Am. Chem. Soc.* **2005**, *127*, 3650–3651.

(52) Escalera-Moreno, L.; Baldoví, J. J.; Gaita-Ariño, A.; Coronado, E. Spin States, Vibrations and Spin

Relaxation in Molecular Nanomagnets and Spin Qubits: A Critical Perspective. *Chem. Sci.* **2018**, *9*, 3265–3275.

(53) Drozdov, A.; Kuzmina, N. Volatile Compounds of Lanthanides. *Compr. Inorg. Chem. II* **2013**, 511–534.

(54) Bedoya-Pinto, A.; Miralles, S. G.; Vélez, S.; Atxabal, A.; Gargiani, P.; Valvidares, M.; Casanova, F.; Coronado, E.; Hueso, L. E. Interface-Assisted Sign Inversion of Magnetoresistance in Spin Valves Based on Novel Lanthanide Quinoline Molecules. *Adv. Funct. Mater.* **2018**, *28*, 1702099.

TABLE OF CONTENTS

We present two families of thermally robust lanthanoid quinolinate coordination complexes. The sodium salt of $[Dy(5,7\text{-}ClIq)_4]^-$, with single-molecule magnet behavior in bulk, is sublimable under gentle conditions. It retains its molecular integrity and the SMM behavior in the sublimated film.